Making Sticky-Slippery Switchable Fluorogels Through Self-Adaptive Bicontinuous Phase Separation

Xiaoxia Li, Baohu Wu, Shengtong Sun, and Peiyi Wu**

Developing gel materials with tunable frictional properties is crucial for applications in soft robotics, anti-fouling, and joint protection. However, achieving reversible switching between extreme sticky and slippery states remains a formidable challenge due to the opposing requirements for energy dissipation on gel surfaces. Herein, a self-adaptive bicontinuous fluorogel is introduced that decouples lubrication and adhesion at varying temperatures. The phase-separated fluorogel comprises a soft fluorinated lubricating phase and a stiff yet thermal-responsive load-bearing phase. At ambient temperature, the fluorogel exhibits a highly slippery surface owing to a low-energy-dissipating lubricating layer, demonstrating an ultralow friction coefficient of 0.004. Upon heating, the fluorogel transitions into a highly dissipating state via hydrogen bond dissociation, concurrently releasing adhesive dangling chains to make the surface highly sticky with an adhesion strength of ≈362 kPa. This approach provides a promising foundation for creating advanced adaptive materials with on-demand self-adhesive and self-lubricating capabilities.

1. Introduction

Material surfaces can exhibit either slippery or sticky behavior by regulating their frictional properties against contacting object.[1] For instance, articular cartilage serves as a slippery hydrogel layer in animal joints that can withstand substantial loads while maintaining an exceptionally low friction coefficient (≈0.001–0.01).[2,3] In contrast, pressure-sensitive adhesives firmly adhere to various solid surfaces through simple contact under normal pressure.[4] Developing materials capable of dynamically switching between slippery and sticky states could significantly enhance their adaptability to changing environments, promising in applications like controlled movement, climbing robotics, anti-fouling, self-cleaning, and joint protection. Toward this goal, researchers have explored materials with tunable frictional properties in response to various stimuli such as temperature,[5–7] light,[8–11] solvent,[12–14] pH,[15] magnetic field,[16] electrical field,[17,18] strain,[19] pressure,[20] and shear force.[21] However, current reports mainly focused on transitions between high and low lubrication or adhesion states (see Table S1, Supporting Information). Rare studies can achieve the switchable friction between extremely slippery and sticky states, largely limiting their advanced adaptive applications.

Friction is a complex process involving energy dissipation as two surfaces slide against each other.[2] Achieving high lubrication requires minimizing frictional energy dissipation while maximizing it promotes adhesion. According to the two-term non-interacting model, frictional energy comprises contributions from both interfacial friction and material deformation.[6,22,23] Consequently, slippery surfaces can be engineered by incorporating thin hydration/lubricant layers and/or increasing bulk stiffness to reduce energy loss during sliding.[6,24–26] Conversely, enhancing interfacial interactions and material deformability can significantly increase interfacial and cohesive energy, leading to high adhesion.[14,27] However, polymer surfaces typically exhibit fixed properties with limited changes in response to environmental conditions. While reversible screening of adhesive groups on thermal-responsive hydrogels has been explored for stick-slip transitions, the achieved amplitude was still restricted due to insufficiently variable energy dissipation mechanisms.[28] Reconciling these opposing factors to achieve dramatic and reversible switching between lubrication and adhesion remains a formidable challenge.

To tackle this issue, in this paper, we introduce a novel strategy of self-adaptive bicontinuous phase separation to decouple lubrication and adhesion at different temperatures. Notably, bicontinuous phase separation, characterized by two interpenetrating continuous phases, provides an ideal platform for integrating diverse components to precisely manipulate material properties.[29–32] Experimentally, we designed a copolymer fluorogel composed of 2-perfluorohexyl ethyl acrylate (PFHEA) and acrylic acid (AA) using perfluoropolyether (PFPE) oligomer as the lubricating solvent (**Figure 1**,b). In this fluorogel, PPFHEA

X. Li, S. Sun, P. Wu
State Key Laboratory for Modification of Chemical Fibers and Polymer Materials
College of Chemistry and Chemical Engineering & Center for Advanced Low-dimension Materials
Donghua University
2999 North Renmin Road, Shanghai 201620, China
E-mail: shengtongsun@dhu.edu.cn; wupeiyi@dhu.edu.cn
B. Wu
Jülich Centre for Neutron Science (JCNS) at Heinz Maier-Leibnitz Zentrum (MLZ) Forschungszentrum Jülich
Lichtenbergstr. 1, 85748 Garching, Germany

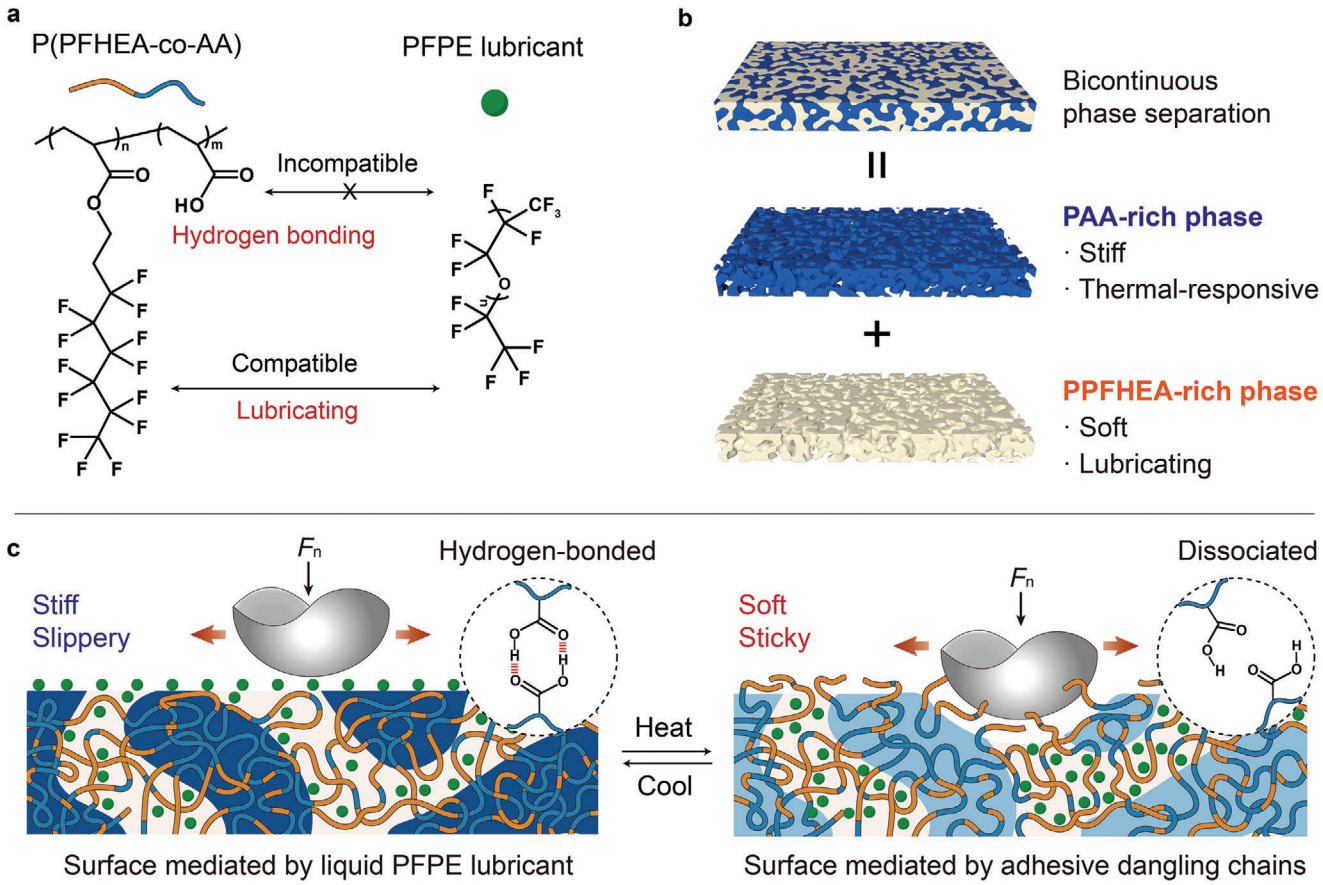

Figure 1. Molecular design and working mechanism of the sticky-slippery switchable fluorogel. a) Chemical structures of the fluorogel comprising P(PFHEA-*co*-AA) copolymer and PFPE lubricant. b) Schematic structure for the polymerization-induced bicontinuous phase separation. The PAA-rich phase serves as a stiff load-bearing component and regulates frictional properties, while the PPFHEA-rich phase functions as a soft lubricating component by confining PFPE lubricant. c) Schematic working mechanism of self-adaptive bicontinuous phase separation for switching between sticky and slippery states. At room temperature, the fluorogel exhibits a stiff, slippery surface coated by a thin liquid PFPE lubricant layer. Upon heating, hydrogen bond dissociation within the PAA-rich phase renders the fluorogel soft and sticky with an adhesive dangling chain-dominated surface. This process is fully reversible.

segments are compatible with PFPE, forming a soft lubricating phase. This phase confines the PFPE lubricant within the polymer network, creating a thin yet self-replenishable lubricating layer on the fluorogel surface. Conversely, PAA segments are incompatible with PFPE but can self-associate through hierarchical hydrogen bonds to form the load-bearing phase. At room temperature, the fluorogel exhibits a highly physical crosslinked structure through hydrogen bonds, resulting in a stiff network and a slippery surface dominated by liquid PFPE lubricant (Figure 1c). These combined low-energy-dissipating effects contribute to an ultralow friction coefficient of 0.004, even under high-speed shear conditions. Upon heating, hydrogen bonds partially dissociate, leading to significantly reduced modulus and increased energy dissipation. Concurrently, the fluorogel surface becomes mediated by adhesive dangling chains, enabling facile penetration into the opposing surfaces.[33] As a result, the fluorogel exhibits strong adhesion with a maximum probe-tack adhesion strength of 362 kPa. Intriguingly, this strong adhesion can be maintained upon cooling without detaching the adherend, demonstrating a high lap-shear adhesion strength of ≈3.8 MPa on a copper substrate. Furthermore, the fluorogel is optically transparent, mechanically tough, anti-fouling, and capable of self-healing, showcasing its great potential for on-demand self-adhesive and self-lubricating applications.

2. Results and Discussion

2.1. Synthesis and Optimization of Bicontinuous Fluorogel

The bicontinuous P(PFHEA-*co*-AA) fluorogel was readily synthesized through photo-initiated copolymerization of PFHEA and AA in the presence of PFPE lubricant. The molar fraction of AA varied from 0 to 60 mol% (relative to total monomer) for recipe optimization, while the volume fraction of PFPE was fixed to 20 vol.%. Notably, PFPE oligomer was chosen as the lubricating solvent due to its low volatility, low surface energy, and universal repellency to various liquids, properties commonly exploited in liquid-infused slippery materials.[19,34,35] As shown in **Figure 2**a,b, the neat PPFHEA/PFPE fluorogel exhibited exceptional softness and elasticity, characterized by a Young's modulus of 29 kPa

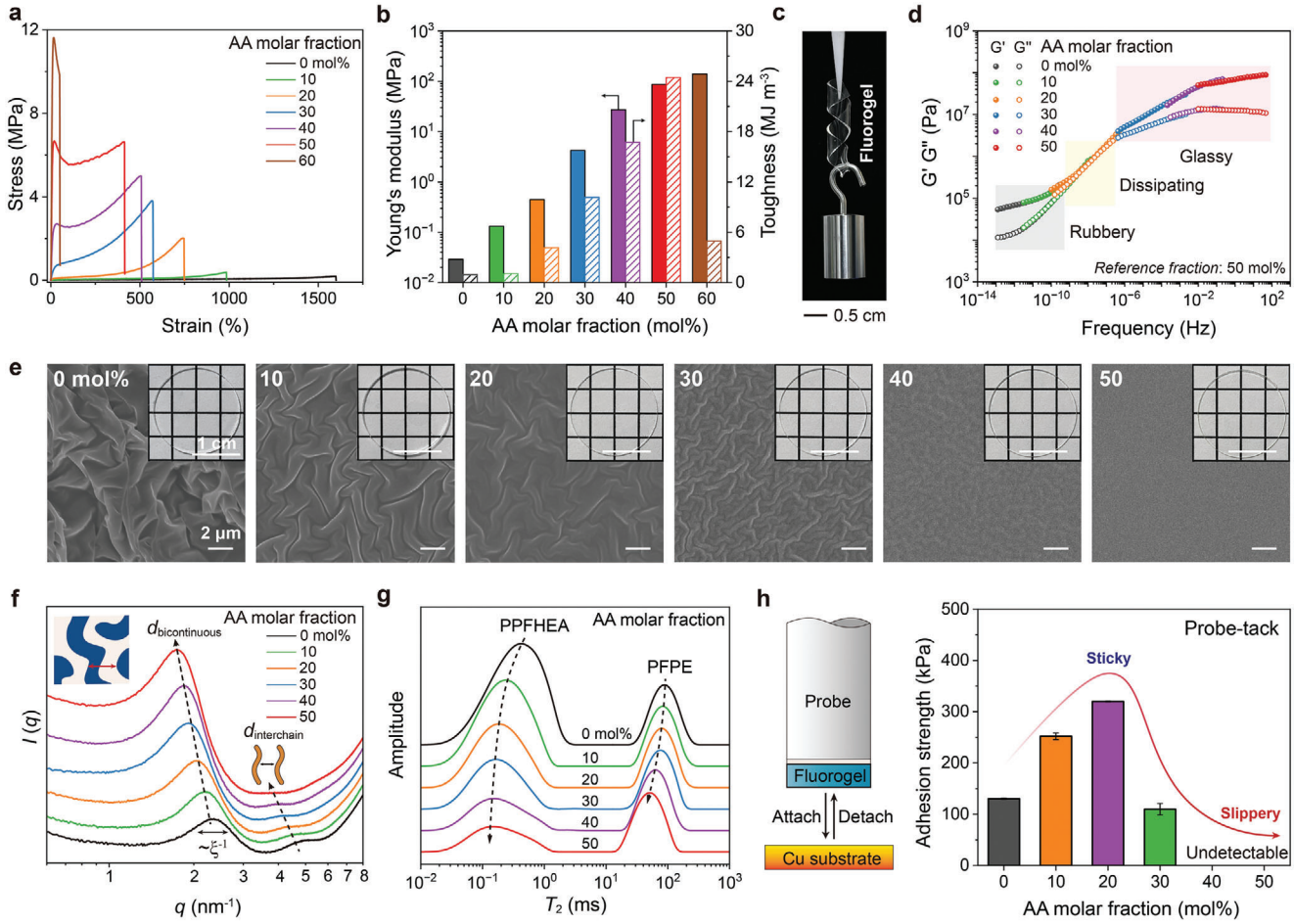

Figure 2. Mechanical properties, structural characterization, and frictional performance of copolymer fluorogels. a) Tensile stress-strain curves of the copolymer fluorogels with increasing AA molar fractions (strain rate: 0.35 s^{-1}). b) Corresponding Young's moduli and toughness. c) Photo of a twisted copolymer fluorogel film with 50 mol% AA supporting a heavy load (50 g). d) Time-fraction superposition rheological master curves (reference fraction: 50 mol% AA). e) Photos and SEM images of fluorogels with increasing AA molar fractions. f) SAXS profiles of the copolymer fluorogels at 20 °C. g) Low-field ^{19}F NMR spectra at 20 °C. h) Schematic set-up for probe-tack adhesion test and the measured adhesion strength.

and an elongation of 1600%. Increasing the AA fraction from 10 to 50 mol% led to a significant enhancement in both modulus and toughness of the copolymer fluorogel. While the fluorogel with 50 mol% AA displayed a reduced elongation (413%), it demonstrated remarkable robustness with a Young's modulus of 86.5 MPa and a maximum toughness of 24.5 MJ m^{-3}. The exceptional load-bearing capacity of this fluorogel was highlighted by its ability to support a weight in its twisted form (Figure 2c). However, at an AA fraction of 60 mol%, the precursor became turbid, and the resulting copolymer displayed inhomogeneous and brittle characteristics (Figure S1, Supporting Information), which will not be discussed in this paper.

Time-fraction superposition rheology was employed to characterize the rheological behavior of different fluorogels at room temperature (Figure 2d; see original data in Figure S2, Supporting Information). The obtained frequency-sweep master curves are characteristic of amorphous polymers, exhibiting three distinct viscoelastic regimes.[14,36] A clear transition was observed from a rubbery regime for 0–10 mol% AA to a dissipating (or glass transition) regime for 20 mol% AA, culminating in a glassy regime for 30–50 mol% AA. This evolution coincided with the emergence of yield points in the tensile curves for AA fractions exceeding 30 mol%, typical for glassy polymers (Figure 2a). The observed trend can be attributed to the progressive strengthening of hydrogen bonding among PAA segments, resulting in an increased physical crosslinking density and restricted segmental mobility.[37] Accordingly, the glass transition temperatures (T_g) determined by both temperature-sweep rheology and differential scanning calorimetry (DSC) exhibited a significant increase with increasing AA molar fractions (Figures S3, S4, Supporting Information).

Besides, all the investigated fluorogels demonstrated remarkable optical transparency, maintaining ~94% transmittance across the visible spectrum, regardless of AA fraction variations (Figure 2e, Figure S5, Supporting Information). However, surface topology, a critical factor influencing lubrication and adhesion performance, varied with increasing AA fractions, as observed by scanning electron microscopy (SEM). Removal of the thin PFPE layer under a high vacuum revealed a collapsed surface of the neat PPFHEA fluorogel, indicating its soft and deformable

nature. Fluorogels with 10–40 mol% AA displayed similar wrinkled textures, albeit with decreasing wrinkle sizes as the AA fraction increased. In contrast, the fluorogel with 50 mol% AA presented a relatively smooth and uniform surface. These findings suggest that the deformability of the soft PPFHEA/PFPE phase was effectively suppressed only when the AA fraction reached 50 mol%.

To elucidate the microstructural evolution of the fluorogels with increasing AA fractions, small-angle X-ray scattering (SAXS) and low-field ^{19}F NMR measurements were conducted. As shown in Figure 2f, the neat PPFHEA fluorogel exhibited a prominent correlation peak centered around $q \approx 2.4$ nm^{-1}, accompanied by a secondary peak near $q \approx 4.8$ nm^{-1}. The low-q peak, indicative of a classic two-phase bicontinuous structure, enabled the extraction of phase-to-phase distance ($d_{\text{bicontinuous}}$, characteristic of periodicity in size) and correlation length (ξ, the dispersion of $d_{\text{bicontinuous}}$) through Teubner-Strey model fitting.[38,39] The peak width is proportional to the reciprocal correlation length ξ^{-1}. The already existing bicontinuous phase separation in the neat PPFHEA fluorogel can be attributed to the chemical incompatibility of the hydrocarbon backbone of PPFHEA with its perfluorinated side chains and PFPE.[36,40] The incorporation of incompatible PAA segments further improved the regularity of bicontinuous phase separation, as evidenced by the increase in ξ from 2.1 to 2.8 nm. Moreover, with increasing AA fractions, the correlation peak shifted toward lower q values, corresponding to an increase in phase-to-phase distance from 2.6 nm for the neat PPFHEA fluorogel to 3.5 nm for the copolymer fluorogel with 50 mol% AA. All these findings unequivocally support the presence of a bicontinuous structure and the ordered expansion of the PAA-rich phase with increasing AA fractions. Furthermore, the secondary peak in the high q regime, ascribed to the interchain distance between PPFHEA chains within the lubricating phase, broadened and eventually vanished as the PAA-rich phase enveloped the entire network. This indicates a gradual weakening in the coupling correlation of soft PPFHEA chains, consistent with the loss of overall chain flexibility as the AA fraction increased.

We further measured the spin-spin relaxation time (T_2) signals by low-field ^{19}F NMR spectra to probe the mobility distribution of F-containing components within the fluorogel (Figure 2g). A higher T_2 value generally correlates with a higher mobility of corresponding species.[14,41] In this system, the lower T_2 peak originates from the fluorinated side chains of PPFHEA, while the higher T_2 peak is attributed to PFPE. As the AA fraction increased, both T_2 peaks shifted toward lower relaxation times, indicating the progressively restricted mobility within PPFHEA/PFPE lubricating phase. Furthermore, low-field NMR T_2 relaxometry is highly sensitive to molecular-scale heterogeneity with different local and long-range spatial mobility of polymer chains.[42,43] This allows for the quantitative analysis of network structure and defects involving free, dangling, and cross-linking chains. By fitting the low-field ^{19}F NMR T_2 spectrum of the fluorogel, we determined the proportions of these three types of chains (Figure S6, Supporting Information). The proportion of dangling chains decreased substantially from 39% in the neat PPFHEA fluorogel to 8% in the copolymer fluorogel with 50 mol% AA, while the proportion of cross-linking chains exhibited an opposite trend. These findings clearly demonstrate that increasing AA fraction leads to a significant enhancement in physical crosslinking density through the formation of additional hydrogen bonds.

The surface frictional properties of the copolymer fluorogels were then evaluated using probe-tack tests (Figure 2h). By applying a constant pressure (40 kPa) for one min, the peak detachment force was measured to determine the adhesion strength on a copper substrate (Figure S7, Supporting Information). The neat PPFHEA fluorogel exhibited a relatively high adhesion strength of 130 kPa, suggesting that despite the presence of PFPE lubricant, the fluorogel's deformability and loosely confined PPFHEA chains still contributed to adhesive interactions.[23,33] Increasing AA fraction to 20 mol% further enhanced adhesion strength to a maximum of 320 kPa. This is reasonable because the dissipating state combines high interfacial adaptability with high energy dissipation, benefitting for high adhesion.[14] However, further increasing AA fraction led to a significant decrease in adhesion strength, with almost no detectable adhesion force for the copolymer fluorogels with 40 and 50 mol% AA, corresponding to highly slippery surfaces. In these cases, the surface was dominated by a thin liquid PFPE lubricant film and tightly crosslinked chains, resulting in negligible energy dissipation from both interface and bulk deformation.

Collectively, the aforementioned characterizations indicate that 50 mol% AA fraction optimizes the desired self-lubricating surface properties at room temperature. At this composition, the copolymer fluorogel is located in a glassy state, demonstrating an ultrahigh modulus and toughness. Furthermore, the fluorogel is transparent and possesses a regular bicontinuous phase-separated structure with a short phase-to-phase distance of only 3.5 nm. This architecture facilitates the nanoconfinement of the PPFHEA-rich lubricating phase within the stiff PAA-rich phase, minimizing the exposure of adhesive dangling chains. These combined effects contribute to an exceptionally slippery surface with negligible adhesion to other substrates. Unless otherwise specified, all subsequent fluorogel samples refer to the AA fraction of 50 mol%.

2.2. Sticky-Slippery Switchable Properties

Owing to the presence of a thermal-responsive PAA-rich phase that adaptively regulates both stiffness and surface topology, the copolymer fluorogel can reversibly switch its sticky and slippery properties at different temperatures. Probe-tack tests were again conducted to evaluate the adhesion strength of the fluorogel on a copper substrate in response to temperature variations. As the temperature increased, the initially slippery surface gradually transitioned to a sticky state with increasing adhesion strength (**Figure 3**a). A maximum adhesion strength of 362 kPa was observed at 80 °C, approaching its glass transition temperature ($T_g \approx 88.3$ °C), where the fluorogel is located in the dissipating state (Figure S3, Supporting Information). This adhesion strength significantly surpasses that of previous stick-slip switchable hydrogels relying on screening adhesive groups (≈30 kPa).[28] Further increasing temperature led to a decrease in adhesion strength as the fluorogel transitioned to the rubbery state, characterized by a reduced modulus and cohesive strength.

Intriguingly, the high adhesion can be maintained upon cooling if the adherend was not removed from the fluorogel.

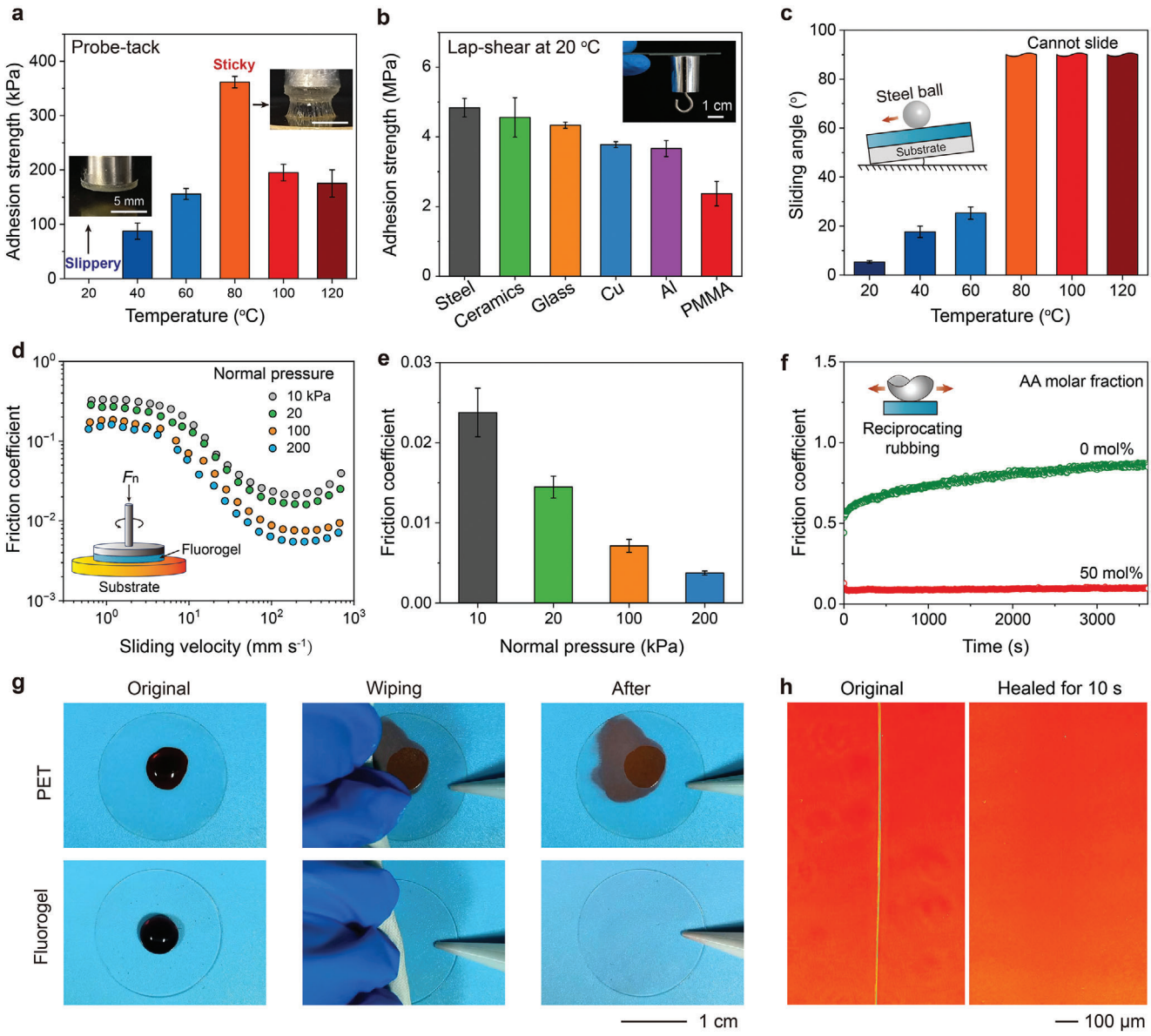

Figure 3. Sticky-slippery switching properties of the copolymer fluorogel with 50 mol% AA. a) Adhesion strength of the fluorogel on a copper substrate at different temperatures (insets show the detaching processes at 20 and 80 °C, respectively). b) Lap-shear adhesion strength of the thermally cured fluorogel on various substrates at 20 °C. c) Sliding angles of a steel ball (7 g) on the fluorogel at different temperatures. d) Sliding velocity-dependent friction coefficients of the fluorogel under different normal pressures. e) Normal pressure-dependent friction coefficients at a sliding velocity of 200 mm s^{-1}). f) Time-resolved friction coefficient variations during 12000 cycles of reciprocating rubbing for the copolymer and neat PPFHEA fluorogels (load: 1 N; slide velocity: 10 mm s^{-1}). g) Photos for wiping the dye solutions (Congo red) on PET and fluorogel films. h) Photos demonstrating the rapid self-healing process of the fluorogel surface at 150 °C.

The lap-shear adhesion strength on a copper substrate reached ca. 3.8 MPa, comparable to many strong cured adhesives (Figure 3b).[41,44–46] This exceptional adhesion also extended to other substrates, such as steel, ceramic, glass, aluminum, and polymethyl methacrylate (PMMA). Notably, even after immersion in water for 24 h, the adhesion strength remained above 2 MPa, attributed to the hydrophobic nature of the fluorogel's fluorinated chains (Figure S8, Supporting Information). We highlight that this property renders the fluorogel particularly suitable for self-adhesive and self-lubricating applications. For instance, a hot fluorogel can be directly applied to robotic joints for high adhesion, and subsequent cooling rapidly restores the self-lubricating properties on the exposed surface, thereby reducing frictional forces during movements.

We further evaluated the heat-induced slippery-to-sticky switching properties of the fluorogel by measuring sliding angles (Figure 3c; Movie S1, Supporting Information). A steel ball (7 g) was employed to simulate a heavy load, mimicking the high-pressure conditions characteristic of articular cartilage. At 20 °C, the fluorogel surface exhibited an ultralow sliding angle of

5°, demonstrating its exceptional slippery performance. The increasing temperature gradually elevated the sliding angle. Above 80 °C, the sliding angle could not be determined as the steel ball completely adhered to the sticky fluorogel, even at an inclination of 90°.

To investigate the normal pressure- and velocity-dependent lubricating properties of the fluorogel at room temperature, friction coefficients were measured by a rheometer. As depicted in Figure 3d,e, the friction coefficient remained low under the tested conditions, while exhibiting a significant reduction with increasing normal pressure and sliding velocity. As discussed above, the low friction coefficient can be attributed to the fluorogel's rigidity and bicontinuous structure, which effectively resist deformation and build interfacial PFPE lubrication. Moreover, a higher pressure facilitated the extrusion of PFPE lubricant from the fluorogel, and increased sliding velocity promoted the transition from boundary to hydrodynamic lubrication, both resulting in reduced friction.[23,25] At a high pressure of 200 kPa and a high velocity of 200 mm s^{-1}, the fluorogel achieved a minimal friction coefficient of 0.004, comparable to that of articular cartilage (≈0.001–0.01).[2,3] We further evaluated the wear resistance of the fluorogel upon reciprocating rubbing for 12000 cycles (Figure 3f). The rigid copolymer fluorogel maintained a stable low friction coefficient throughout the entire process, demonstrating its excellent wear resistance. In contrast, the soft and sticky neat PPFHEA fluorogel exhibited a significantly higher friction coefficient that also continuously increased over wearing time.

The excellent slippery property also brings good anti-fouling properties for the copolymer fluorogel. For demonstration, a Congo red dye solution was dropped onto both fluorogel and polyethylene terephthalate (PET) films as a control. While the dye adhered permanently to the PET surface despite multiple wipes, it exhibited minimal adhesion to the slippery fluorogel, allowing complete removal (Figure 3g; Movie S2, Supporting Information). Furthermore, the fluorogel can self-heal its surface when abraded or damaged by sharp objects. For instance, a scar inflicted on the fluorogel surface by a knife completely vanished after heating at 150 °C for only 10 s (Figure 3h). This excellent healing property is attributed to the fluorogel's reconfigurable network enabled by the heat-induced dissociation of hydrogen bonds as dynamic physical crosslinkers.[47–50]

2.3. Mechanism Discussion for Self-Adaptive Bicontinuous Phase Separation

To elucidate the underlying mechanism governing the fluorogel's sticky-slippery switching properties at the nano- and molecular scales, we conducted a series of temperature-dependent characterizations, including rheology, low-field ^{19}F NMR, SAXS, and IR spectroscopy. We first plotted the rheological master curves for the fluorogel following the time-temperature superposition principle at a reference temperature of 20 °C (**Figure 4a**). As temperature increased or frequency decreased, the fluorogel transitioned from a glassy state to a dissipating and rubbery states, consistent with previous analyses. In the dissipating state, a pronounced tan δ peak emerged around 80 °C, accompanied by a high loss modulus (G″) of 0.6 MPa, indicative of its high energy dissipation for optimal adhesion. To further probe the distribution of relaxation modes, rheological data were converted into relaxation spectra, $H(\tau)$, using the generalized Maxwell model (Figure 4b).[41] Compared to the neat PPFHEA fluorogel (see rheological master curves in Figure S9, Supporting Information), both glass transition and rubbery relaxation modes of the copolymer fluorogel shifted toward longer relaxation times, suggesting the enhanced chain confinement due to the formation of hydrogen-bonded physical crosslinks. This enhanced confinement is further supported by a significant elevation in activation energy from 85.1 kJ mol^{-1} for the neat PPFHEA fluorogel to 202.9 kJ mol^{-1} for the copolymer fluorogel (Figure 4c; see calculation in Figure S10, Supporting Information). Notably, a new relaxation mode attributed to PAA emerged in the relaxation spectrum of the copolymer fluorogel, corroborating the presence of a well-defined PAA-rich phase in the bicontinuous structure.

Temperature-variable low-field ^{19}F NMR spectra were acquired to monitor the mobility changes of the PPFHEA and PFPE components in the fluorogel (Figure 4d). As the temperature increased, PFPE mobility was enhanced, while the PPFHEA signal split into two peaks above 80 °C. The emerging higher shoulder peak for PPFHEA is attributed to the released dangling chains resulting from the dissociation of hydrogen bonds among PAA segments. Notably, upon cooling, peak changes were fully reversible, demonstrating the excellent structural reversibility of the fluorogel. To further quantify these changes, the proportions of free, dangling, and cross-linking chains were calculated at different temperatures (Figure 4e). While increasing temperature induced only a slight reduction in free chains, a dramatic increase in dangling chains at the expense of cross-linking chains was observed. The cooling process reversed all these proportional changes. These findings clearly reveal that the high adhesion of the fluorogel at elevated temperatures is directly correlated with the presence of adhesive dangling chains, whereas the high lubrication at room temperature is attributed to a high proportion of cross-linking chains.

To investigate phase structural changes accompanying the temperature-induced slippery-to-sticky transition, temperature-variable SAXS measurements were conducted (Figure 4f). Notably, the correlation peak associated with bicontinuous phase separation remained constant at q = 1.7 nm^{-1}, indicating minimal structural alterations during the heating process. This suggests that the bicontinuous structure did not change significantly in the heating process. However, a discernible intensity change was observed in the scattering patterns below and above q = 2.2 nm^{-1}, attributed to bicontinuous phase separation and chain entanglement, respectively. Apparently, increasing temperature led to the dissociation of more hydrogen bonds, resulting in reduced phase contrast and the formation of longer polymer chains prone to topological entanglements.[37]

To gain deeper insights into the molecular changes associated with self-adaptive bicontinuous phase separation, temperature-variable transmission IR spectra of the copolymer fluorogel were recorded from 25 to 120 °C (Figure 4g). We focused on the C═O stretching vibrations, which include the spectral information from both the ester groups (COOR) of PPFHEA segments (≈1736 cm^{-1}) and the carboxylic acid groups (COOH) of PAA segments (≈1710 cm^{-1}). Heat induced the dissociation of both dimeric and oligomeric hydrogen bonds within PAA segments, as evidenced by the reduced intensity of corresponding peaks.

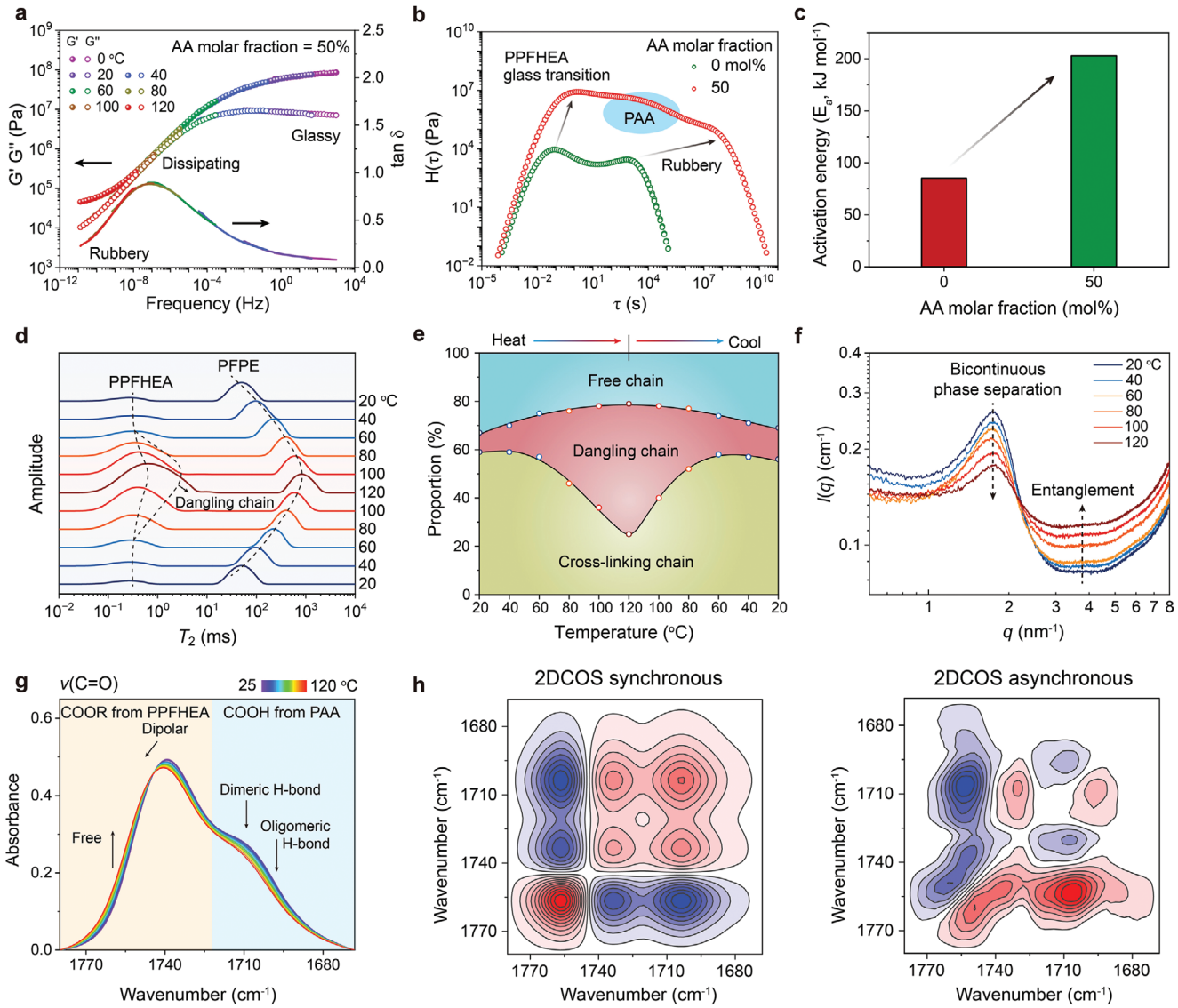

Figure 4. Mechanism analysis for the self-evolving bicontinuous phase separation in the copolymer fluorogel with 50 mol% AA. a) Time-temperature superposition rheological curves of the copolymer fluorogel at a reference temperature of 20 °C. b) Rheological relaxation spectra of neat PPFHEA fluorogel (0 mol% AA) and the copolymer fluorogel. c) Calculated activation energies. d) Low-field ^{19}F NMR spectra of the copolymer fluorogel upon heating from 20 to 120 °C and subsequent cooling to 20 °C. e) Calculated proportions of free, dangling, and cross-linking chains at different temperatures. f) Temperature-variable SAXS profiles. g) Temperature-variable transition IR spectra of the fluorogel upon heating from 25 to 120 °C (interval: 10 °C). h) 2DCOS synchronous and asynchronous spectra generated from (g). In 2DCOS spectra, red colors represent positive intensities, while blue colors represent negative intensities.

Concurrently, a transition from dipolar to free ester groups was observed for PPFHEA segments.

Two-dimensional correlation spectroscopy (2DCOS) was further employed to extract more subtle information about interaction changes within the fluorogel (Figure 4h). Synchronous and asynchronous spectra were generated to reflect synchronized and unsynchronized changes in spectral intensities at specific wavenumbers, respectively. Based on Noda's judging rule (see determination details in Table S2, Supporting Information),[37,51,52] the responsive order of different C=O groups to heat was determined as follows: 1749 cm^{-1} → 1730 cm^{-1} → 1761 cm^{-1} → 1697 cm^{-1} → 1738 cm^{-1} → 1707 cm^{-1} (→ means prior to or earlier than), corresponding to ν(COOH) (free, PAA) → ν(C=O) (strongly dipolar, PPFHEA) → ν(C=O) (free, PPFHEA) → ν(COOH) (oligomeric hydrogen bond, PAA) → ν(C=O) (weakly dipolar, PPFHEA) → ν(COOH) (dimeric hydrogen bond, PAA). The earliest response of COOH-related changes suggests that heat-induced chain dynamics in the fluorogel were primarily driven by the hydrogen bond dissociation of PAA segments. Consequently, an increased number of PPFHEA-rich dangling chains are exposed on the fluorogel surface, enhancing interfacial adhesion. This process also led to a higher PAA content on the fluorogel surface at 80 °C compared to 20 °C, as detected by ATR-FTIR spectral comparison (Figure S11, Supporting Information).

Due to the incompatibility of PAA with PFPE, the increased PAA content on the surface of the fluorogel would force the PFPE lubricant into the interior. As a result, the formation of a PFPE lubricant layer was suppressed at elevated temperatures.

The aforementioned characterizations together support the proposed mechanism of self-adaptive bicontinuous phase separation for regulating sticky-slippery switching properties (Figure 1c). At the nanoscale, the heat did not disrupt the bicontinuous structure, which maintained a distinct separation between the thermal-responsive PAA-rich phase and the lubricating PPFHEA-rich phase. However, at the molecular level, heat-induced the partial dissociation of hydrogen bonds within PAA segments, releasing polymer chains to enhance chain entanglement and generating adhesive dangling chains that promoted interfacial penetration. These combined effects contributed to ultrahigh energy dissipation arising from both interfacial friction and material deformation, culminating in high adhesion near the glass transition temperature.

3. Conclusion

In this paper, we report a new strategy for achieving dramatic and reversible switching between lubrication and adhesion through temperature-triggered adaptive bicontinuous phase separation. This approach relies on decoupling energy dissipation mechanisms that are typically antagonistic for these two frictional states. To prove this concept, we synthesized a bicontinuous copolymer fluorogel with intertwined two phases: a soft lubricating phase and a stiff yet thermal-responsive load-bearing phase. At ambient temperature, the fluorogel exhibited a highly slippery surface due to a confined liquid lubricant layer. Conversely, upon heating, the fluorogel underwent a dramatic transition to a highly sticky state. While the bicontinuous structure remained largely intact, the underlying molecular changes are pivotal. Heat-induced dissociation of hydrogen bonds within the thermal-responsive phase led to network softening, enhancing bulk energy dissipation, and the release of adhesive dangling chains, which boosted interfacial energy dissipation. Notably, the fluorogel also combined transparency, robustness, anti-fouling, and self-healing capabilities, demonstrating its potential for transformative applications in on-demand self-adhesive and self-lubricating systems.

Supporting Information

Supporting Information is available from the Wiley Online Library or from the author.

Acknowledgements

The authors gratefully acknowledge the financial support from the National Natural Science Foundation of China (NSFC) (Nos. 52322306, 21991123, 22275032, 52161135102). S.S. also thanks the support from the Shanghai Oriental Talent Program and Talent Development Fund (No. 2021021).

Conflict of Interest

The authors declare no conflict of interest.

Data Availability Statement

The data that support the findings of this study are available from the corresponding author upon reasonable request.

Keywords

adaptive materials, adhesion, gels, lubrication, phase separation

[1] V. L. Popov, *Contact Mechanics and Friction*, Springer, Berlin **2010**.
[2] W. Lin, J. Klein, *Adv. Mater.* **2021**, *33*, 2005513.
[3] S. Jahn, J. Klein, *Macromolecules* **2015**, *48*, 5059.
[4] C. Creton, *MRS Bull.* **2003**, *28*, 434.
[5] Y. Ru, R. Fang, Z. Gu, L. Jiang, M. Liu, *Angew. Chem., Int. Ed.* **2020**, *59*, 11876.
[6] Y. Zhang, W. Zhao, S. Ma, H. Liu, X. Wang, X. Zhao, B. Yu, M. Cai, F. Zhou, *Nat. Commun.* **2022**, *13*, 377.
[7] C. Linghu, Y. Liu, Y. Y. Tan, J. H. M. Sing, Y. Tang, A. Zhou, X. Wang, D. Li, H. Gao, K. J. Hsia, *Proc. Natl. Acad. Sci* **2023**, *120*, e2221049120.
[8] J. Wang, X. Zhang, S. Zhang, J. Kang, Z. Guo, B. Feng, H. Zhao, Z. Luo, J. Yu, W. Song, S. Wang, *Matter* **2021**, *4*, 675.
[9] F. Wang, M. Liu, C. Liu, Q. Zhao, T. Wang, Z. Wang, X. Du, *Sci. Adv.* **2022**, *8*, eabp9369.
[10] D. Kim, H. Kim, W. Jeon, H. J. Kim, J. Choi, Y. Kim, M. S. Kwon, *Adv. Mater.* **2024**, *36*, 2309891.
[11] J. Liu, Y. S. Huang, Y. Liu, D. Zhang, K. Koynov, H. J. Butt, S. Wu, *Nat. Chem.* **2024**, *16*, 1024.
[12] H. Cho, G. Wu, J. C. Jolly, N. Fortoul, Z. He, Y. Gao, A. Jagota, S. Yang, *Proc. Natl. Acad. Sci* **2019**, *116*, 13774.
[13] J. Xiong, M. Duan, X. Zou, S. Gao, J. Guo, X. Wang, Q. Li, W. Li, X. Wang, F. Yan, *J. Am. Chem. Soc.* **2024**, *146*, 13903.
[14] Y. Shi, B. Wu, S. Sun, P. Wu, *Adv. Mater.* **2024**, *36*, 2310576.
[15] L. Hu, Y. Yang, J. Hao, L. Xu, *Nano Lett.* **2022**, *22*, 6004.
[16] W. Wang, J. V. I. Timonen, A. Carlson, D. M. Drotlef, C. T. Zhang, S. Kolle, A. Grinthal, T. S. Wong, B. Hatton, S. H. Kang, S. Kennedy, J. Chi, R. T. Blough, M. Sitti, L. Mahadevan, J. Aizenberg, *Nature* **2018**, *559*, 77.
[17] J. Huang, Y. Liu, Y. Yang, Z. Zhou, J. Mao, T. Wu, J. Liu, Q. Cai, C. Peng, Y. Xu, B. Zeng, W. Luo, G. Chen, C. Yuan, L. Dai, *Sci. Robot.* **2021**, *6*, eabe1858.
[18] J. Kang, X. Zhang, X. Yang, X. Yang, S. Wang, W. Song, *Adv. Mater.* **2023**, *35*, 2307705.
[19] X. Yao, Y. Hu, A. Grinthal, T. S. Wong, L. Mahadevan, J. Aizenberg, *Nat. Mater.* **2013**, *12*, 529.
[20] H. Zhao, Q. Sun, X. Deng, J. Cui, *Adv. Mater.* **2018**, *30*, 1802141.
[21] X. Zhang, J. Wang, H. Jin, S. Wang, W. Song, *J. Am. Chem. Soc.* **2018**, *140*, 3186.
[22] F. P. Bowden, D. Tabor, *The Friction and Lubrication of Solids*, Oxford University Press, New York **2001**.
[23] Y. Zhang, W. Zhao, X. Zhao, J. Zhang, B. Yu, S. Ma, F. Zhou, *Friction* **2024**, *12*, 1757.
[24] M. Rong, H. Liu, M. Scaraggi, Y. Bai, L. Bao, S. Ma, Z. Ma, M. Cai, D. Dini, F. Zhou, *Adv. Funct. Mater.* **2020**, *30*, 2004062.
[25] Y. Ru, Y. Yang, Q. Wu, R. Fang, T. Zhao, J. Klein, M. Liu, *Angew. Chem., Int. Ed.* **2023**, *62*, 202302765.
[26] J. Huang, Y. Tang, P. Wang, H. Zhou, H. Li, Z. Cheng, Y. Wu, Z. Xie, Z. Cai, D. Wu, H. Shen, *Adv. Mater.* **2024**, *36*, 2309141.

[27] H. Yuk, T. Zhang, S. Lin, G. A. Parada, X. Zhao, *Nat. Mater.* **2016**, *15*, 190.
[28] Z. Zhang, C. Qin, H. Feng, Y. Xiang, B. Yu, X. Pei, Y. Ma, F. Zhou, *Nat. Commun.* **2022**, *13*, 6964.
[29] M. Wang, P. Zhang, M. Shamsi, J. L. Thelen, W. Qian, V. K. Truong, J. Ma, J. Hu, M. D. Dickey, *Nat. Mater.* **2022**, *21*, 359.
[30] C. Fernández-Rico, S. Schreiber, H. Oudich, C. Lorenz, A. Sicher, T. Sai, V. Bauernfeind, S. Heyden, P. Carrara, L. D. Lorenzis, R. W. Style, E. R. Dufresne, *Nat. Mater.* **2024**, *23*, 124.
[31] H. Ye, B. Wu, S. Sun, P. Wu, *Adv. Mater.* **2024**, *36*, 2402501.
[32] L. Zeng, Y. Fu, H. Cui, Y. Zhao, Y. Liu, X. Lin, T. Chao, H. Guo, *Adv. Funct. Mater.* **2024**, *34*, 2407397.
[33] N. Maeda, N. Chen, M. Tirrell, J. N. Israelachvili, *Science* **2002**, *297*, 379.
[34] X. Yao, S. S. Dunn, P. Kim, M. Duffy, J. Alvarenga, J. Aizenberg, *Angew. Chem., Int. Ed.* **2014**, *53*, 4418.
[35] L. Yang, S. Dong, W. Zhou, Q. Wu, Y. Zheng, J. Cui, *Chem. Eng. J.* **2021**, *417*, 127901.
[36] H. Xiang, X. Li, B. Wu, S. Sun, P. Wu, *Adv. Mater.* **2023**, *35*, 2209581.
[37] H. Ye, B. Wu, S. Sun, P. Wu, *Nat. Commun.* **2024**, *15*, 885.
[38] M. Teubner, R. Strey, *J. Chem. Phys.* **1987**, *87*, 3195.
[39] C. Frank, H. Frielinghaus, J. Allgaier, H. Prast, *Langmuir* **2007**, *23*, 6526.
[40] J. Wang, G. Mao, C. K. Ober, E. J. Kramer, *Macromolecules* **1997**, *30*, 1906
[41] H. Qiao, B. Wu, S. Sun, P. Wu, *J. Am. Chem. Soc.* **2024**, *146*, 7533.
[42] G. Simon, K. Baumann, W. Gronski, *Macromolecules* **1992**, *25*, 3624.
[43] V. M. Litvinov, R. A. Orza, M. Klüppel, M. van Duin, P. C. M. M. Magusin, *Macromolecules* **2011**, *44*, 4887.
[44] K. Liu, P. Wu, *Angew. Chem., Int. Ed.* **2024**, *63*, 202403220.
[45] J. Zhang, X. Zhou, Q. Hu, K. Zhou, Y. Zhang, S. Dong, G. Zhao, S. Zhang, *Nat. Commun.* **2024**, *15*, 4265.
[46] S. Chen, Q. Guo, J. Yu, *Aggregate* **2022**, *3*, e293.
[47] M. J. Webber, M. W. Tibbitt, *Nat. Rev. Mater.* **2022**, *7*, 541.
[48] Q. Du, P. Wu, S. Sun, *Fundam. Res.* **2024**, https://doi.org/10.1016/j.fmre.2024.05.008.
[49] Y. Huang, C. Peng, Y. Li, Y. Yang, W. Feng, *Aggregate* **2023**, *4*, e319.
[50] J. Qi, T. Wu, W. Wang, H. Jin, S. Gao, S. Jiang, J. Huang, Y. Yan, *Aggregate* **2022**, *3*, e173.
[51] W. Zhang, B. Wu, S. Sun, P. Wu, *Nat. Commun.* **2021**, *12*, 4082.
[52] S. Sun, P. Wu, *Chin. J. Polym. Sci.* **2017**, *35*, 700.